Internal Spatial Modes in Glass Microring Resonators

Gregory H. Vander Rhodes, Bennett B. Goldberg, M. Selim Ünlü, *Senior Member, IEEE*, Sai-Tak Chu, and Brent E. Little, *Member, IEEE*

***Abstract*—We have used near-field scanning optical microscopy to measure the internal optical modes inside glass waveguides and microring resonators. The period of the observed standing modes provides a direct measure of the local effective index. The measured effective index and modal shape determines the values of all components of the wave vector. The observed standing modes inside the ring resonator are unexpected, but are caused by the standing modes in the coupling waveguide. Last, we describe a technique that can obtain detailed information about the locations of the dielectric interfaces.**

***Index Terms*—Channel drop filter, integrated optics, near-field scanning optical microscopy, ring resonator.**

I. Introduction

In THE near future, large-scale integrated optical systems with densely packed simple optical components will constitute the building blocks of optical communication networks and signal processing circuits. These all-optical circuits are faster, more scalable, and potentially less expensive than their hybrid electrical/optical analogs since there is no need to perform optical to electrical conversion. Precise modeling and exacting fabrication of dielectrical structures are necessary to build the next generation of integrated optical systems. Also essential are new techniques for accurate characterization of such optical systems, from the most basic building blocks like simple channel waveguides to novel structures such as microring resonators for wavelength-division multiplexing (WDM).

A variety of characterization techniques have been developed for probing guided-wave devices [1]. Transmission measurements, the most basic of these techniques, treat the device as a "black box," providing direct information about its operation as a whole unit, like switching characteristics and temperature stability. Extending transmission measurements with a wavelength tunable source provides additional data about the operation of wavelength sensitive devices, as well as about Fabry–Perot cavities within the component under test.

Transmission measurements give global information about the entire device and as such are very suitable for determining qualitative device performance. Unfortunately, transmission and reflectivity measurements are not very effective for diagnostic purposes, since the causes of most device problems are local and microscopic within the device. Traditional far-field microscopy can identify spatially certain device limitations, for instance, loss due to absorption or scattering. On the other hand, if the problem can be traced to the internal operation of the device, such as undesired multimoded behavior, far-field microscopy is fruitless. Common techniques for modal analysis, such as prism out-coupling [2] and exit facet imaging [3], cannot generally identify local problems resulting in unwanted modal structure.

It is therefore essential to develop a way of probing internal spatial modes within these guided-wave devices. Several methods have been used to measure internal optical fields, all of which depend on converting a fraction of the guided wave into far-field radiation. One method is to dope or coat the device with a light sensitive material, as has been demonstrated using Er^{+} doping [4] and photoluminescence enhanced polymers [5]. The doped or coated device will then emit light into the far-field in proportion to the local intensity of the guided wave. A second method uses a device made of a uniformly scattering material such as poly-Si to scatter the guided light into the far field [6], but this method is generally only a side-effect, not applicable to most high-quality devices. In this paper, we will show that near-field scanning optical microscopy can be used to measure internal optical intensity within both basic and novel guided-wave structures. We will show that this method has a number of advantages over the methods above, including the ability to distinguish scattered from guided light and determine the vectoral components of the wavevector, all with a minimum amount of perturbation.

II. Near-Field Scanning Optical Microscopy

Near-field scanning optical microscopy [7], [8] (NSOM) raster scans a tapered single-mode fiber-optic [9] serially, building up a high-resolution image of a sample. The aperture in the tapered fiber is much less than the wavelength of light and therefore, when scanned in close proximity to the sample, yields an image with resolution better than the diffraction limit. The earlier development of NSOM has targeted applications where ultrahigh spatial resolution was required [10]. More recently, NSOM has been recognized as a tool to study evanescent fields to obtain otherwise inaccessible information about guided-wave optical systems. NSOM studies of waveguides have demonstrated evanescent field decay [11], standing modes [12], [13], and recently observed a modulation in the propagation direction [14] due to the Tien effect [15]. Studies of more complicated devices have included directional couplers [16] and star couplers [14]. We have demonstrated the first

Manuscript received July 6, 1999. This work was supported in part by the National Science Foundation under Grant ECS-9 625 236 and Grant DMR-9413855 and by the Department of Education under Grant P200A50267-97.

G. H. Vander Rhodes, B. B. Goldberg, and M. S. Ünlü are with the Department of Physics and the Department of Electrical and Computer Engineering, Boston University Photonics Center, Boston, MA 02215-2421 USA.

S.-T. Chu is with the Kanagawa Academy of Science and Technology, Kawasaki-shi, Kanagawa 213 Japan.

B. E. Little is with the Research Laboratory of Electronics, Massachusetts Institute of Technology, Cambridge, MA 02139 USA.

Publisher Item Identifier S 1077-260X(00)01146-1.

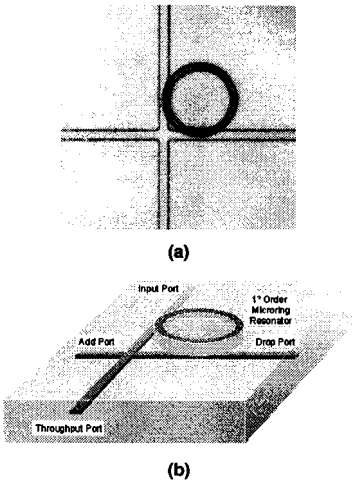

Fig. 1. (a) Optical micrograph of a glass microring resonator and buried crossed bus waveguides. (b) Schematic of device structure, showing the buried waveguides and identifying the various ports.

modal characterization of single mode optical waveguides with direct measurements of the propagation vector components and standing wave structures [13]. This paper presents a detailed characterization and analysis of guided wave devices by NSOM. In the following section, we describe the optical waveguide and microring resonator structures that we studied.

III. Device Under Test

Optical channel drop filters separate different wavelength optical signals and are therefore of enormous interest in WDM networks. An early design for a channel drop filter is two bus waveguides side-coupled to a ring resonator between them. This was first proposed in the late 1960's [17] but fabricated many years later [18]. The side-coupled geometry presents a number of challenges for fabrication, generally requiring the use of electron-beam lithography to define the desired separation and coupling coefficient between the bus waveguides and the ring. The device studied here, shown in Fig. 1, is unique in that the ring resonator is *vertically* coupled to the bus waveguides, which puts the crucial parameter in the growth direction, allowing for much more accurate control of the thickness and thus the coupling coefficient [19]. The devices studied employ cross-bus waveguides, which provide for easy cascading in a $1 \times N$ or $N \times N$ geometry in a very small wafer area [20]. Last, these microring resonators are fabricated in a low-index material system, which is not only better matched to silica fibers but is also more forgiving of sidewall roughness.

In the fabricated device, alternating layers of SiO_2 and the compound glass Ta_2O_5/SiO_2 were deposited by RF sputtering. The processing consisted of the following steps. An initial layer of 10–μm-thick SiO_2 was deposited on the Si substrate to serve as the bottom cladding layer. This was followed by the deposition of a 0.5–μm layer of Ta_2O_5/SiO_2. A 150-nm-thick Cr mask was evaporated on to the sample and subsequently patterned by photolithography and dry etched to a depth of 0.5 μm, forming the bus waveguide core. While the Cr on top of the bus waveguides remained intact, 0.5 μm of SiO_2 was sputtered onto the sample to fill in the amount of Ta_2O_5/SiO_2 material etched away.

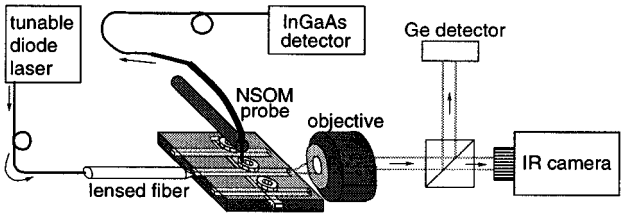

Fig. 2. Experimental setup used for characterizing internal optical fields inside guided-wave devices. Light from tunable laser is launched into the device under test, and the transmitted light is analyzed. The NSOM probe is scanned over the surface of the device, measuring both topography and sampling the evanescent field.

In the Cr liftoff process, the sample was first soaked in BHF for 10 s to remove the SiO_2 deposited on the vertical walls of the Cr. Thus exposed, the Cr was subsequently wet etched, which lifted both the Cr and the SiO_2 on top of it. A buffer layer of SiO_2, the depth of which determines the vertical separation of the bus and ring waveguides, was next sputtered onto the sample. Last, a 1-μm-thick top layer of Ta_2O_5 was deposited and subsequently patterned with a Cr mask to form the air-clad ring waveguide structure.

IV. Waveguide Studies

The bus waveguides underneath the microring resonator are simple channel waveguides. Analytical or numerical solutions of the optical modes are easily obtained. This simplicity makes them an ideal testbench for initial NSOM studies, providing proof of the characterization technique.

A schematic of our setup is shown in Fig. 2. A lensed fiber is used to launch light from a tunable external cavity laser into the guided-wave device under study. Transmitted light at the exit facet is imaged onto both a charge-coupled device for optimizing coupling and a Ge photodiode for quantitative measurements. The NSOM probe is scanned over the surface of the waveguide, routing the collected light to an InGaAs photodetector. The translation stage used to scan the tip is interferometrically calibrated to ±0.3 nm, and a shear-force tuning fork method [21] is used during surface scans to maintain a tip-surface separation of 10 nm.

As mentioned in the introduction, a standard technique of characterization is transmission spectroscopy. Fig. 3 shows a transmission spectrum for the waveguide, at a frequency far from any ring resonances. The oscillations are due to the cavity formed by the entrance and exit facets. The measured free spectral range (FSR) of 0.096 nm yields a cavity length of 9 mm, identical to the length of the sample. The measured peak-to-valley ratio of 1.02 is much lower than expected from the reflectivities of the entrance and exit facets. This is likely due to the detection of unguided light since we did not use a pinhole in the exit image plane.

If a large amount of scattering is present, the field at the surface will not be simply related to the internal modes. A vital initial measurement in this and similar studies is a comparison of the level of scattered light to the evanescent field at the surface [22]. The measured optical intensity from NSOM scans in the vertical plane, perpendicular to the direction of light propagation, is plotted in Fig. 4(a) above the schematic of the structure.

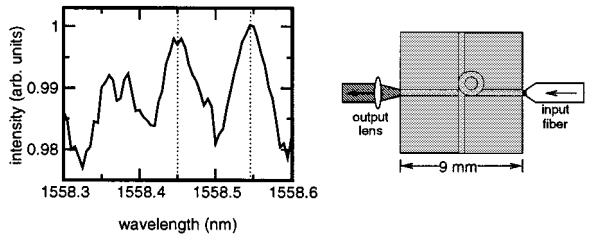

Fig. 3. (a) Transmission spectrum for the waveguide by itself, away from any ring resonances. The distance between the two dotted lines is 0.096 nm, the FSR of a 9-mm cavity. (b) Schematic of the device, identifying the 9-mm cavity.

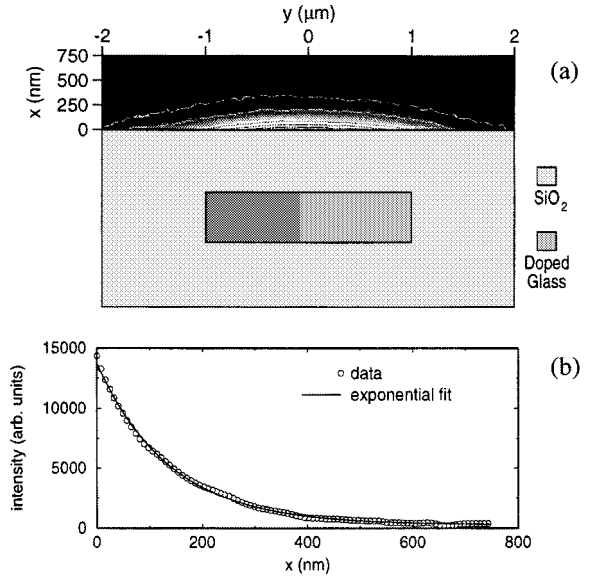

Fig. 4. (a) Measured optical intensity from NSOM scans in the vertical plane, shown on top of a schematic cross section of the waveguides under study. Grayscale map uses black to indicate zero intensity and white for high intensity. Contours are added to enhance visibility of features. A complete decay of the field at a height(x) of around 500 nm is observed. (b) Line cut taken from above at $y = 0$, with exponential fit with intensity decay coefficient $(2\alpha_x) = 7.34\ \mu\text{m}^{-1}$.

The intensity decays quickly as a function of height showing the absence of scattering into free-space propagating modes. A vertical line-cut of this data, shown in Fig. 4(b), exhibits pure exponential behavior, consistent with theoretical simulations. The value for the exponential decay constant α_x obtained from Fig. 4(b) is ~20% smaller than the value predicted by finite difference time-domain (FDTD) simulations. This is due to the metal-coated NSOM tip and will be discussed in detail later.

In Fig. 5(a), we use the NSOM probe to observe a slight ridge on the surface above the buried waveguide core. The sample above the bus is designed to be planar, but the fabrication tolerances allow for a variation in height of a few nanometers between the side cladding and core. The observed ridge allows us to spatially anchor our optical scans. The actual width of the surface structure does not directly correspond to the buried waveguide dimension since the ridge may not propagate vertically as the top cladding layer is grown.

A large variation with polarization is observed in the NSOM optical scans, because the measured waveguides are not designed for polarization insensitive operation. When TM modes

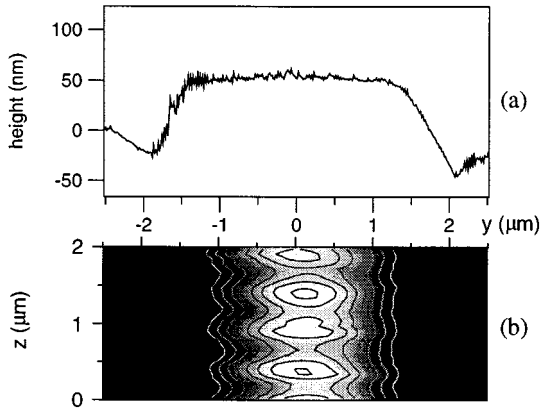

Fig. 5. (a) Line scan of the surface topography across the waveguide, showing ridge at surface due to buried waveguide. (b) Optical image obtained at the surface of the waveguide when TM modes are excited. The periodic variation in the z direction is a standing mode due to a cavity formed in the waveguide. A line cut for $y = 0$ exhibits almost pure sinusoidal behavior, with a peak-to-valley ratio of 1.2.

are excited by controlling the input polarization, we obtain the image shown in Fig. 5(b). The dependence along y of the measured optical intensity is consistent with a single-mode waveguide. The periodic variation in the $\hat{z}$-direction is the standing wave due to the cavity formed between the entrance and exit facets of the waveguide. The peak-to-valley ratio along $\hat{z}$ is ~10%, consistent with the entrance and exit facet reflectivities. The period of the standing mode is given by $\lambda_0/2n_{\text{eff}}$, where λ_0 is the vacuum wavelength and n_{eff} is the effective index for the guided optical mode. The measured $n_{\text{eff}} = 1.458$ compares very favorably with simulations, which yield $n_{\text{eff}} = 1.473$. Since our scanning stages are interferometrically calibrated, the small difference between data and simulation actually provides a more accurate measure of the waveguide dimensions than those initially supplied to the simulation.

The traditional method of solving a rectangular waveguide assumes that the values of the components of $\vec{k}$, the wave vector, are constant within a region [17]. This assumption, while convenient, leads to unphysical situations, especially at the corners of a rectangular waveguide. In reality, only the component along the propagation direction k_z is constant everywhere in order to satisfy phase matching, while k_x and k_y may vary as long as the dispersion relationship is satisfied: $k_x^2 + k_y^2 + k_z^2 = n^2 k_0^2$, for a material with index n. Along the direction perpendicular to the waveguide surface $\hat{x}$, the propagation constant is imaginary resulting in a evanescent field $(k_x \rightarrow -i\alpha)$. Vertical line cuts of Fig. 2 can be fitted to obtain a reduced value of α as a function of y, across the waveguide, shown in Fig. 6.

A similar behavior of the guided modes is expected for TE polarization with only minor changes in the mode shapes and $\vec{k}$ values. However, an NSOM scan for TE [Fig. 7(a)] is dramatically different—note the off-center peak. The design wavelength of our device is very close to the cutoff condition of the first higher order mode, TE_1. Any slight variation in physical parameters could easily cause the waveguide to become double moded. The off-center peak indicates a significant contribution from TE_1. The fact that the guide is multimoded makes a determination of k_x very difficult, because the fitting of the exponential decay would have to fit weighted amounts of all of the

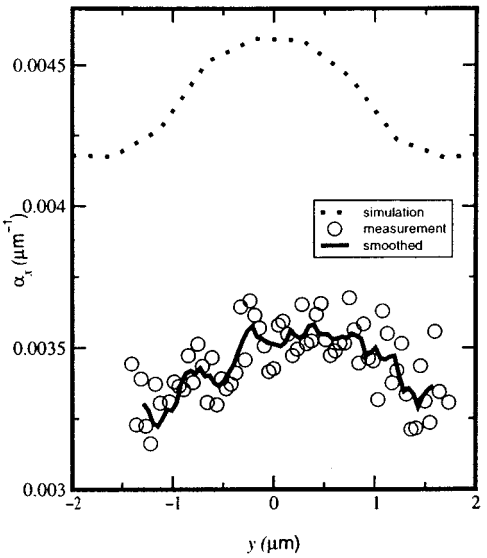

Fig. 6. Measurements and simulations of α_x as a function of y. Due to the noise in the measurement, a smoothed version has been overlaid on the measured data for easier comparison with simulation.

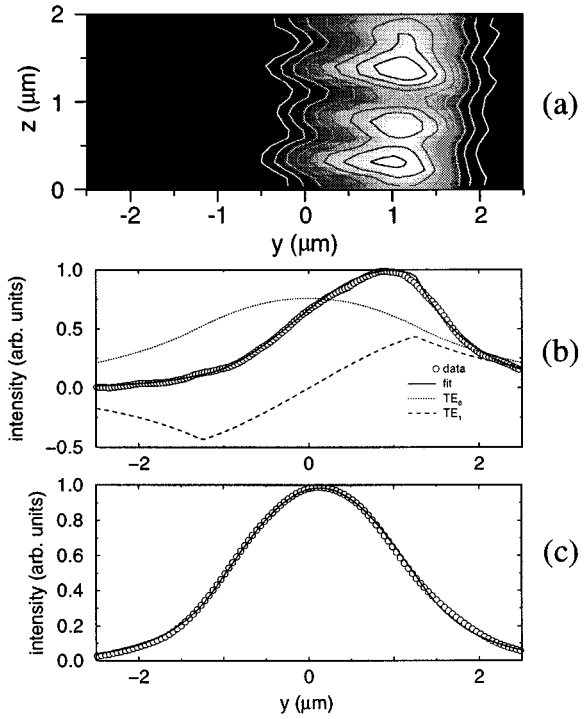

Fig. 7. (a) Optical image obtained at the surface of the waveguide when TE modes are excited. A line cut at $y = 1$ μm exhibits mostly sinusoidal behavior, with a peak-to-valley ratio of 1.3. (b) Intensity line cut of TE image taken at constant z, with a fit consisting of the weighted superposition of TE_0 (59%) and TE_1 (41%), with a phase difference of 0.098 radians. The theoretical solutions are also shown for TE_0 and TE_1. (c) Line cut of TM image, with a fit to the lowest order solution in a step-index waveguide.

decay constants for all of the excited modes. So instead we use an alternative method to obtain the values of the wave vector. The component of $\vec{k}$ across the waveguide k_y can be obtained from the mode shape. Solutions of a step index waveguide give $\cos k_y y$ (even order) or $\sin k_y y$ (odd order) within the core region, with decaying exponentials outside this region. Fig. 7(b) shows a line cut along the y, with a fit to the lowest order solution. The parameters of this fit give k_y and thus k_x in different regions of the waveguide, summarized in Table I. This technique is also applied to the TM modes in Fig. 7(c), though what we are observing is actually an average value for components of $\vec{k}$, since it is not possible to get full y dependence using this fitting technique.

A measurement technique should introduce negligible perturbation to the system under study. From our measurements of the optical modes on the surface, it is clear that this perturbation is small for the purposes of measuring k_z from the period of the standing mode. However, the perturbation is causing a significant change to the measurements of α_x from the exponential decay constant, as mentioned earlier. This perturbation is most likely due to the Al-coating on the NSOM fiber tip, which causes the optical mode within the waveguide to be slightly depressed. The metal coating introduces a new reflecting boundary condition, which causes the local evanescent field under the tip to fall off more slowly than in its absence, giving a reduced value for α_x. The use of uncoated tips appears to give values for α closer to expected [14], and we will be performing these experiments with uncoated tips to confirm this interpretation of the data.

If the probe is indeed modifying the internal optical mode, we should be able to see this effect in the transmission through the waveguide. The amount of light detected by the tip as it is scanned across the waveguide is compared to the amount of light simultaneously transmitted in Fig. 8.

The 1% drop in transmission is correlated exactly to the light collected by the NSOM probe. Two explanations are possible. The first is that the coated probe is causing a change in the effective index of refraction for the guided mode, and that the change in transmission is due to reflection at the probed point. The second explanation is that the transmission drops because

TABLE I
MEASURED PROPAGATION CONSTANTS FOR THE WAVEGUIDE, SHOWN IN VALUES OF μm^{-1}

	TE_0	TM_0	TE_1
α_x	4.352	4.361	4.374
k_y	0.645	0.703	0.783

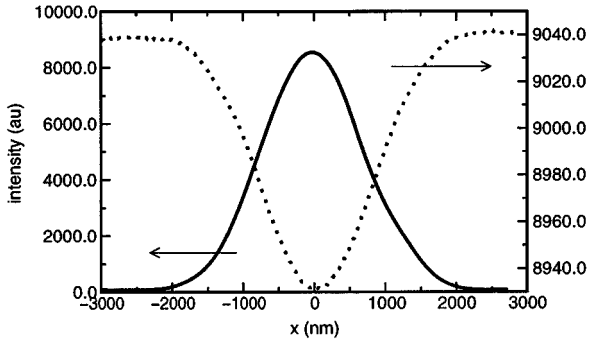

Fig. 8. Signal collected by the NSOM probe (left scale, solid) and light transmitted through the waveguide (right scale, dotted) as a function of lateral distance across the waveguide. When the NSOM probe is collecting light, the transmitted signal is reduced at most by about 1%. Solid line: mode intensity. Dashed line: transmission.

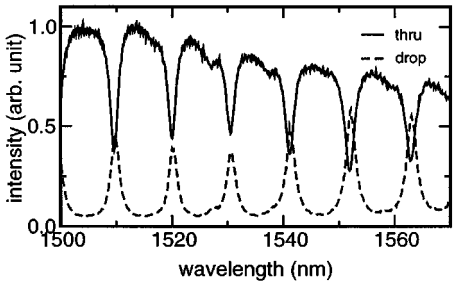

Fig. 9. Transmission spectra through the ring resonator, showing signal at the through port (solid) and drop port (dotted) when light is launched into the input port. The slight drop in the transmission at longer wavelengths is due to the lower responsivity of the Ge detector used.

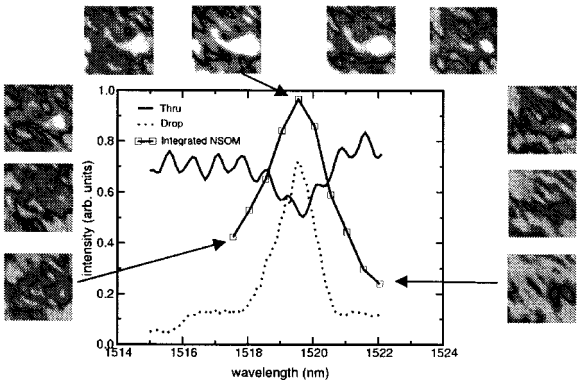

Fig. 10. Comparison of the light stored in the ring resonator to the amount detected at the through and drop ports. The integrated NSOM trace is obtained by performing a 500-nm square scan on the surface of the ring and then summing the pixels. The transmission scans are different from those in Fig. 9 because of the difference in sample orientation.

light is being coupled into the probe, although not all of it can propagate from the aperture to the untapered region. Typical transmission values for pulled tips such as these are between 10^{-4} and 10^{-6}, so it is within reason that we would detect 1 pW using an NSOM probe that is collecting 1% of the 10 μW launched into the waveguide. We will be studying both of these effects further during our comparison of coated versus uncoated tips.

V. Ring Studies

The experimental setup for studying the ring resonator is similar to the setup for measuring the bus waveguide, but with one important addition: a large core multimode fiber optic is mounted to collect light coming out of the drop port. This allows us to monitor both the through and drop port simultaneously with the NSOM scans. Fig. 9 shows normalized transmission spectra from the through and drop ports as a function of input frequency. The device resonates, and light is sent to the drop port as successive integral numbers of wavelengths fit around the ring circumference. Though these particular devices do not possess as high-quality filter characteristics as other reports for similar devices [20], they are quite suitable for our purposes.

Fig. 10 shows a series of small, 500-nm square NSOM scans taken at a fixed location within the ring as a function of frequency across a resonance. Within the plot, the amount of light transmitted through the drop and through ports is compared to

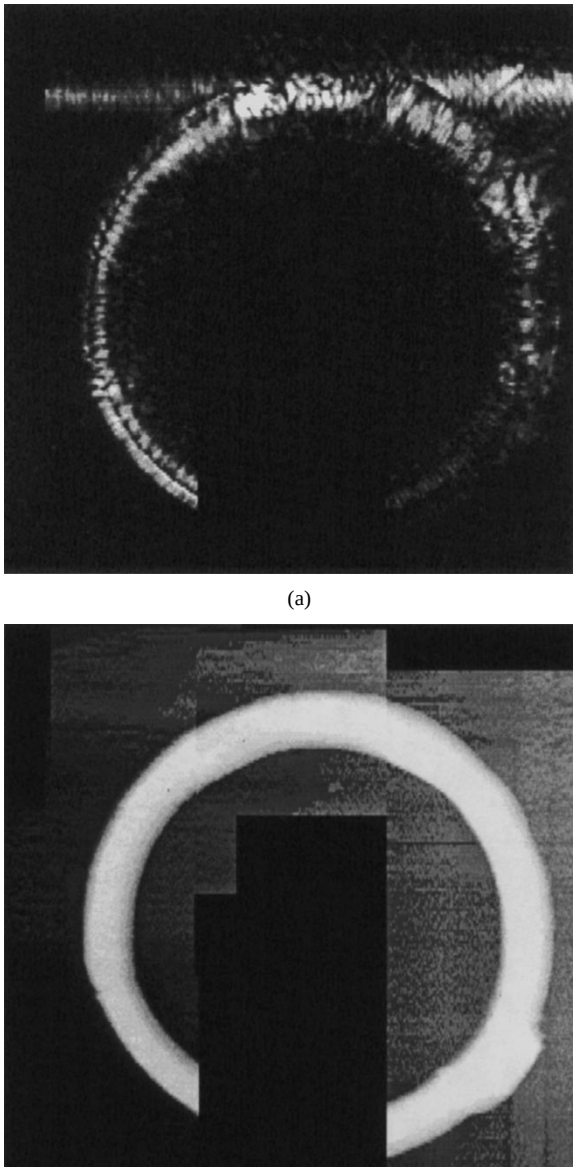

(a)

(b)

Fig. 11. Multiple NSOM scans of the ring resonator, stitched together for an image of almost the entire ring on resonance. Entire scan is 58 μm square. (a) shows the optical modes, clearly showing the light coming into the resonator in the upper right, with about half of that light leaving the resonator at the drop port in the upper left. The launch orientation used here is not especially efficient in coupling to the drop port, which is why very little light is seen at the drop port in the upper right. (b) is topography, with a height difference of 1.45 μm from black to white.

the sum of the total intensity of each image. The similar full-width, half-maximum of these lines confirms that the amount of light stored in the resonator is proportional to the amount routed to the drop port.

Because our scan range is limited, we took multiple NSOM scans and stitched them together electronically, completing an image of almost the entire ring structure with a radius of 25 μm. The orientation of the launch here was different from that for the transmission measurements: rather than launching light into the input port, light was instead launched into the through-port. This alternate launch was done to highlight the interesting phenomena in the ring about the location where the bus waveguides cross. In the NSOM scans in Fig. 11, we observe standing

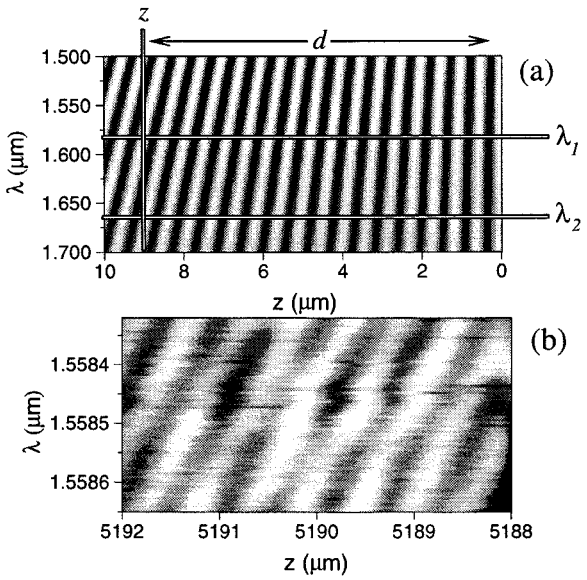

Fig. 12. (a) Simulation of electric field intensity as a function of z and λ for a system with an interface at $z = 0$ μm. The propagation direction is in the $-z$ direction. Variables used to identify d are identified. (b) Experimental results for the waveguide. The interface is again at $z = 0$.

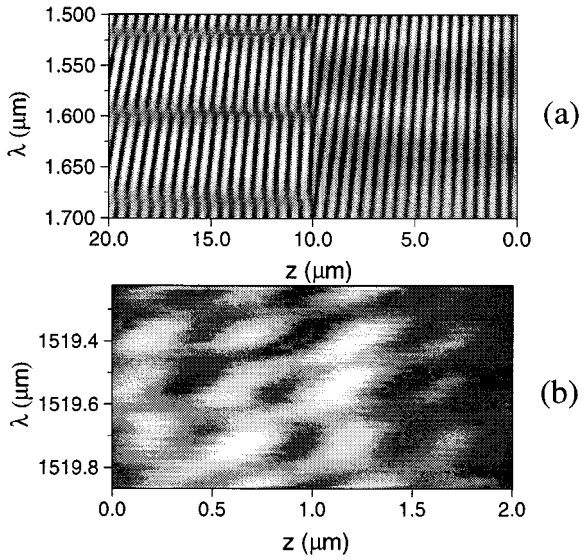

Fig. 13. (a) Simulation of the electric field intensity as a function of z and λ for a system with two interfaces: one at $z = 0$ μm and one at $z = 10$ μm, with the propagation of light in the $-z$ direction. (b) Experimental results for the standing modes in the ring resonator near a resonance wavelength.

modes, which is somewhat unexpected considering the travelling wave nature of the ring resonator. A simulation similar to those in [23] shows standing modes in the ring, but it is important to note that this simulation shows a fixed-time snapshot of the physical system. Because the time scale of the NSOM measurement is many orders of magnitude longer than the time scale of the travelling wave, we expect our measurement to be approximated by a time-averaged FDTD simulation, which has no variation in the angular $(\hat{z})$ direction.

The existence of the standing modes allow for the measurement of n_{eff} and k_z, although the lack of clarity and uniformity in the standing modes disallows the use of this data for any sort of high precision measurements. For the ring standing modes, we obtain a value for the effective index that is about $n_{\text{eff}} = 1.5$, which identifies the modes in the ring as first order, since second-order modes would have a smaller effective index.

Standing modes in a guided-wave structure have their origin in a set of reflectivities that cause a guided-wave to reflect back on itself in an in-phase manner. These reflections may also give rise to additional resonances, which are undesired in the ring structure. Especially since the standing modes in the ring are so unexpected, a useful tool would be one that could identify the location of these reflectivities. In the next section, we explain a technique that can help identify these reflectivities.

VI. Standing Mode Spectroscopy

Transmission measurements can provide information about the overall cavity length, but the absolute position of a dielectric interface or a defect along the waveguide cannot be determined. We have developed a simple and direct measurement that allows for identifying the precise location of any local interface. Fig. 12(a) shows the standing waves formed in the presence of a dielectric interface as a function of wavelength. Note that the slope of the lines formed by the standing waves as a function of the wavelength (λ) decreases for increasing distance from the fixed phase point at $z = 0$, where the slope is infinite. The λ-dependence of the intensity at constant z provides information about the distance d of this measurement point to the output interface given by

$$d = \frac{\pi \lambda_1 \lambda_2}{2(\lambda_1 - \lambda_2)}. \tag{1}$$

To test the accuracy of this technique, we measure the standing mode in the waveguide as a function of wavelength in Fig. 12(b). Using the above analysis, we obtain a distance d of 5.19 mm, correctly matching the distance from the probed region to the exit facet.

Though this is an obvious result, for a more complicated system, this technique can give a wealth of information about various dielectric interfaces. To demonstrate this, in Fig. 13(a) we look instead at the standing modes formed by two interfaces, the first located at zero and the second at 10 μm. In the area after the second interface, we see two very distinct effects. The first is again a decreasing slope with increasing distance from the interface, although the slope is not infinite at the second interface like it is at the first interface. The second effect is a repeating modulation in the standing modes as a function of wavelength. This modulation has the same period as the FSR of the cavity formed between the two interfaces and does not change as a function of distance from the second interface.

Though this system is much simpler than the system of the ring and waveguides, we can still use the intuition gained in Fig. 13(a) to analyze the ring. Just as we did for the waveguide itself, we pick a small region of the standing mode in the ring and scan it as a function of wavelength. The resulting image, shown in Fig. 13(b), looks very similar to the area after the second interface—a repeating modulation on top of lines of a certain slope. The period of the repeating modulation corresponds to a distance of 4.19 mm, identical to the distance between the exit

facet and where the ring intersects with the input-throughput bus waveguide.

One way to think about this system is to unroll it—perfect coupling between the ring and the waveguide would have simply added $2\pi R$ to the length of the overall cavity. However, coupling is incomplete and in fact depends on the strength of the field at the position of the ring. The standing mode in the ring is actually caused by the standing mode in the waveguide and should disappear if the standing mode in the waveguide is eliminated, perhaps by reducing the reflectivity the exit facet. This will be the subject of further experiments.

VII. Summary

We have demonstrated the use of near-field scanning optical microscopy to measure optical intensities on the surface of channel waveguides and microring resonators. Because these structures exhibit very low scattering, these studies represent direct measurement of the internal guided optical modes. Measurements of the exponential decay constant on the surface of the waveguides give a smaller value for α than expected from simulations. We believe this is due to the modification of the internal optical mode by the metal-coated NSOM tip. Observations of standing modes in the waveguides were used to obtain a value for the effective index for the guided wave.

Standing waves in the ring were used to measure the effective index for the guided wave in the ring and identify it as first order. Last, we showed evidence that this unexpected standing wave in the ring was a result of the standing wave in the underlying bus waveguides.

Future experiments will be performed to verify our explanations for the reduced α decay constant and the origin of the standing modes in the ring. We hope to use these NSOM techniques to measure other devices, like new photonic bandgap-based waveguide filters and microcavities, in the hope of directly measuring the small modal volume exhibited in these structures.

References

[1] S. I. Hosain, J. P. Meunier, E. Bourillot, F. de Fornel, and J. P. Goudonnet, "Review of the basic methods for characterizing integrated-optic waveguides," *Fiber Integrated Opt.*, vol. 14, pp. 89–107, 1995.

[2] R. Ulrich and R. Torge, "Measurement of thin film parameters with a prism coupler," *Appl. Opt.*, vol. 12, p. 2901, 1973.

[3] L. McCaughan and E. E. Bergmann, "Index distribution of optical waveguides from their mode profile," *J. Lightwave Technol.*, vol. LT-1, p. 241, 1983.

[4] G. N. van den Hoven, A. Polman, C. van Dam, J. W. M. van Uffelen, and M. K. Smit, "Direct imaging of optical interferences in erbium-doped Al_2O_3 waveguides," *Opt. Lett.*, vol. 21, no. 8, pp. 576–579, Apr. 15, 1996.

[5] D. G. Lidzey, D. D. C. Bradley, M. A. Pate, J. P. R. David, D. M. Wittaker, T. A. Fisher, and M. S. Skolnick, "Mapping the confined optical field in a microcavity via the emission from a conjugated polymer," *Appl. Phys. Lett.*, vol. 71, no. 6, pp. 744–746, Aug. 11, 1997.

[6] D. Rafizadeh, J. P. Zhang, R. C. Tiberio, and S. T. Ho, "Propagation loss measurements in semiconductor microcavity ring and disk resonators," *J. Lightwave Technol.*, vol. 16, pp. 1308–1314, July 1998.

[7] U. Durig, D. W. Pohl, and F. Rohner, "Near-field optical scanning microscopy," *J. Appl. Phys.*, vol. 59, p. 3318, 1986.

[8] M. Paesler and P. Moyer, *Near-Field Optics: Theory, Instrumentation, and Applications*. New York: Wiley, 1996.

[9] E. Betzig, J. K. Trautman, T. D. Harris, J. S. Weiner, and R. L. Kostelak, "Breaking the diffraction barrier: Optical microscopy on a nanometric scale," *Science*, vol. 251, p. 1468, 1991.

[10] B. B. Goldberg, M. S. Ünlü, W. D. Herzog, and E. Towe, "Near field optical microscopy and spectroscopy of heterostructures and laser diodes," *IEEE J. Select. Topics Quantum Electron.*, vol. 1, pp. 1073–1081, 1995.

[11] D. P. Tsai, H. E. Jackson, R. C. Reddick, S. H. Sharp, and R. J. Warmack, "Photon scanning tunneling microscope study of optical waveguides," *Appl. Phys. Lett.*, vol. 56, no. 16, pp. 1515–1517, Apr. 16, 1990.

[12] P. L. Phillips, J. C. Knight, B. J. Mangan, P. St. J. Russell, M. D. B. Charlton, and G. J. Parker, "Near-field optical microscopy of thin photonic crystal films," *J. Appl. Phys.*, vol. 85, no. 9, pp. 6337–6342, May 1, 1999.

[13] G. H. Vander Rhodes, B. B. Goldberg, M. S. Ünlü, S. T. Chu, W. Pan, T. Kaneko, Y. Kokubun, and B. E. Little, , submitted for publication.

[14] S. Bourzeix, J. M. Moison, F. Mignard, F. Barthe, A. C. Boccara, C. Licoppe, B. Mersali, M. Allovon, and A. Bruno, "Near-field optical imaging of light propagation in semiconductor waveguide structures," *Appl. Phys. Lett.*, vol. 73, no. 8, pp. 1035–1037, Aug. 24, 1998.

[15] P. K. Tien, J. P. Gordon, and R. Whinnery, "Light waves in thin films and integrated optics," *Proc. IEEE*, vol. 53, p. 129, 1965.

[16] A. G. Choo, H. E. Jackson, U. Thiel, G. N. D. Brabander, and J. T. Boyd, "Near field measurements of optical channel waveguides and directional couplers," *Appl. Phys. Lett.*, vol. 65, no. 8, pp. 947–949, Aug. 22, 1994.

[17] E. A. J. Marcatelli, "Dielectric rectangular waveguide and directional coupler for integrated optics," *Bell Syst. Tech. J.*, vol. 48, pp. 2071–2102, 1969.

[18] S. C. Hagness, D. Rafizadeh, S. T. Ho, and A. Taflove, "FDTD microcavity simulations: Design and experimental realization of waveguide-coupled single-mode ring and whispering-gallery-mode disk resonators," *J. Lightwave Technol.*, vol. 15, pp. 2154–2165, Nov. 1997.

[19] B. E. Little, S. T. Chu, W. Pan, D. Ripin, T. Kaneko, Y. Kokubun, and E. P. Ippen, "Vertically coupled glass microring resonator channel dropping filters," *IEEE Photon. Technol. Lett.*, vol. 11, pp. 215–217, Feb. 1999.

[20] S. T. Chu, B. E. Little, W. Pan, T. Kaneko, S. Sato, and Y. Kokubun, "An eight-channel add-drop filter using vertically coupled microring resonators over a cross grid," *Photon. Technol. Lett.*, vol. 11, pp. 691–693, June 1999.

[21] K. Karrai and R. D. Grober, "Piezoelectric tip-sample distance control for near field optical microscopes," *Appl. Phys. Lett.*, vol. 66, no. 14, pp. 1842–1844, 1995.

[22] G. H. Vander Rhodes, M. S. Ünlü, B. B. Goldberg, J. M. Pomeroy, and T. F. Krauss, "Characterization of waveguide microcavities using high-resolution transmission spectroscopy and near-field scanning optical microscopy," *Proc. Inst. Elect. Eng. Optoelectron.*, vol. 37, no. 4, pp. 379–383, Dec. 1998.

[23] B. E. Little, J. S. Foresi, G. Steinmeyer, E. R. Thoen, S. T. Chu, H. A. Haus, E. P. Ippen, L. C. Kimerling, and W. Greene, "Ultra-compact Si-SiO2 microring resonator optical channel dropping filters," *Photon. Technol. Lett.*, vol. 10, pp. 549–551, Apr. 1998.

Gregory H. Vander Rhodes was born in Pittsburgh, PA, in 1971. He received the B.S. degree from Carnegie-Mellon University, Pittsburgh, in 1993 and the M.A. degree from Boston University, Boston, MA, in 1995, both in physics. He currently is pursuing the Ph.D. degree in the Near-Field Microscopy Laboratory at Boston University.

His research interests include guided-wave devices, photonic bandgap structures, and novel characterization techniques for these and other photonic devices.

Bennett B. Goldberg was born in Boston, MA, in 1959. He received the B.A. degree from Harvard College, Cambridge, MA, in 1982, and the M.S. and Ph.D. degrees in physics from Brown University, Providence, RI, in 1984 and 1987, respectively.

Following a Bantrell postdoctoral appointment at the Massachusetts Institute of Technology and the Francis Bitter National Magnet Lab, he joined the physics Faculty at Boston University in 1989, where his is now an Associate Professor of physics and of electrical, computer, and systems engineering. His current research interests include low- and room-temperature near-field scanning optical microscopy and spectroscopy in semiconductors and biological systems; magneto-optics and magneto-transport of low-dimensional electron systems; spectroscopy of wide-gap III–V nitrides; and ultrasensitive waveguide biosensors.

Prof. Goldberg has been a member of APS, MRS, and LEOS.

M. Selim Ünlü (S'90–M'92–SM'95) was born in Sinop, Turkey, in 1964. He received the B.S. degree from Middle East Technical University, Ankara, Turkey, in 1986 and the M.S.E.E. and Ph.D. degrees from the University of Illinois, Urbana-Champaign, in 1988 and 1992, respectively, all in electrical engineering.

His dissertation topic dealt with resonant cavity enhanced photodetectors and optoelectronic switches. From 1984 to 1986, he was a part-time Research Engineer with Military Electronics, Inc., Ankara, where he worked on VHF communication systems. In 1992, he joined the Department of Electrical and Computer Engineering, Boston University, Boston, MA, as an Assistant Professor. He has been an Associate Professor there since 1998. His current research interests include design, fabrication, characterization, and modeling of semiconductor optoelectronic devices, near-field and picosecond spectroscopy, integrated optical biosensors, and optical pumping for production of hyperpolarized Xe for MRI.

During 1994–1995, Dr. Ünlü was Chair of the IEEE Laser and Electro-Optics Society, Boston Chapter, winning the LEOS Chapter-of-the-Year Award. He also received the United Nations TOKTEN award in 1995 and 1996 and NSF-CAREER and ONR Young Investigator Awards in 1996. He is currently Vice President of the SPIE New England Chapter.

Sai-Tak Chu, photograph and biography not available at the time of publication.

Brent E. Little (S'87–M'89), photograph and biography not available at the time of publication.